Task 5: Discussion and Modeling

In this section, we discuss the results of the corrosion testing and the oxide characterization and draw conclusions regarding the objectives of the program, namely:

- to demonstrate a technical basis for the improvement of the corrosion resistance of zirconium-based alloys in more extreme operating environments (such as those present in severe fuel duty cycles (high burnup, boiling, aggressive chemistry) and
- to investigate the feasibility (from the corrosion point of view) of using advanced zirconium-based alloys in a supercritical water environment.

This technical basis is obtained through the comparison of the corrosion kinetics and the examination of the fine structure of oxide layers formed on model alloys. These model alloys are designed to isolate specific features of the microstructure that are thought to affect the formation of the protective oxide layer. The key aspect of the program is to rationalize the differences in corrosion kinetics between alloys through the differences in the structure and evolution of the protective oxide formed on each alloy.

Overall Corrosion Performance during Corrosion Testing at 360ºC

As shown in Section 2, the corrosion performance of the Zr alloys in this study varied widely, both among precipitate forming and solid solution forming alloys. Figure 5.1 shows the corrosion weight gain for a representative group of precipitate-forming Zr alloys tested in 360ºC water and Figure 5.2 shows the same plot for solid solution alloys.

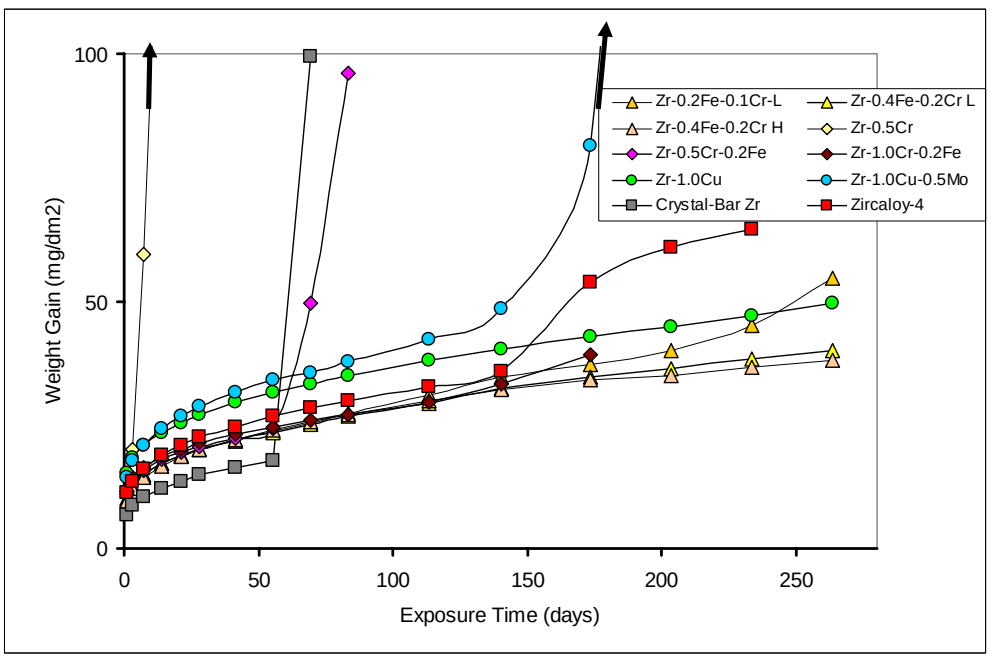

Figure 5.1: Weight gain vs. exposure time for precipitate-forming model alloys tested in 360 ^{o}C water.

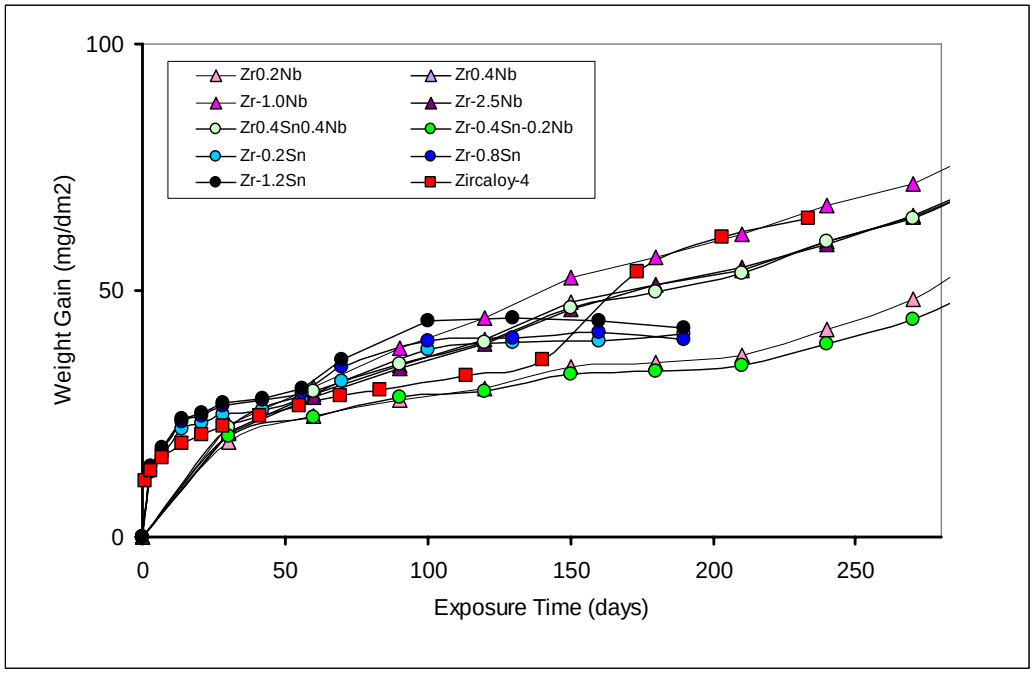

Figure 5.2: Corrosion weight gain for Zr-Nb, Zr-Nb-Sn and Zr-Sn model alloys tested in 360 ^{o}C pure water.

Significant differences are observed in the corrosion behavior of the various alloys. These differences manifest themselves both in the tendency to exhibit breakaway behavior and in the clear separation of the value of the exponent n among the various alloys.

A few important points are listed below:

1. Several alloys, especially in the ZrFeCr system, showed protective behavior with stable oxide growth in all environments for the duration of the test.
2. Oxides formed in alloys with extensive solid solutions (especially Zr-Nb) did not show either obvious transitions or breakaway behavior.
3. The onset of breakaway was not directly related to the pre-breakaway oxide growth kinetics.
4. Very small amounts of alloying elements make a significant difference in corrosion behavior, as can be seen by comparing the behavior of alloy 12 (Zr0.2Fe0.1Cr (H)) with pure Zr.
5. As the alloying element content increases, the tendency to breakaway decreases, but the effect is not linear. A level of about 0.6% total precipitate-forming alloying element content appears to make the oxide resistant to breakaway.

Overall Corrosion Performance during Corrosion Testing at 500ºC

The overall corrosion performance of the alloys during high temperature testing was better than expected with several alloys surviving the full exposure time. The general

agreement between the three high temperature tests was quite good. In particular little difference was seen between the results from static and dynamic autoclave testing. The results from lower pressure static testing agreed with the supercritical water results but showed slightly less oxide growth. Since the rankings of the alloys were preserved from test to test, it is possible the steam test could serve as a preliminary screening test for supercritical water behavior.

As in low temperature testing, there was wide variation in the behavior of the alloys, and compared to low temperature testing, the corrosion rates were much higher [1]. However the alloys that behaved the best in low temperature testing also behaved well in high temperature testing, i.e. the corrosion rankings were quite similar.

The results suggest that the alloy composition and microstructure are predominant in determining corrosion behavior. In general, the best alloys were from the ZrFeCr system (which also behaved the best in a 360ºC water corrosion test). Higher alloying content (at least above 0.6%) improved corrosion resistance. The key to good corrosion resistance is to avoid breakaway corrosion and to maintain a stable, protective oxide. The onset of breakaway often occurs after long exposure times, which indicates that short exposure tests may be inadequate for determining corrosion behavior at high temperature.

Figure 5.3 shows a comparison of the weight gains for some of the model Zr alloys from this study and for ferritic-martensitic (F-M) and austenitic alloys, also under consideration for the SCWR, tested in supercritical water containing 25 ppb oxygen [2]. It is apparent that the corrosion rates for the best Zr alloys are higher than those seen for austenitics and lower than those seen for ferritic-martensitic alloys. However austenitic alloys exhibit extensive cracking in SCW [3]. In addition, it appears that the oxide growth in the Zr alloys is more stable than in the F-M and austenitic alloys (less incidence of weight loss or sudden weight changes). Figure 5.3 also illustrates that the current Zr-based model alloys have been tested to much longer times than the Fe-based alloys currently under consideration. It should be noted that although the results for the F-M and austenitic alloys are for tests conducted with 25 ppb oxygen, the corresponding results for tests performed in deaerated supercritical water (<10 ppb oxygen) show very similar behavior.

Overall, the oxidation rate of the best Zr alloy at 500ºC is lower than that of the best F-M alloy by about a factor of 2. While significant concerns exist in terms of mechanical properties of Zr alloys at SCW temperatures, this research indicates that proper alloying additions induce protective oxide growth in model Zr alloys. From the corrosion point of view, Zr alloys should be considered as possible candidate materials for application in the supercritical water reactor.

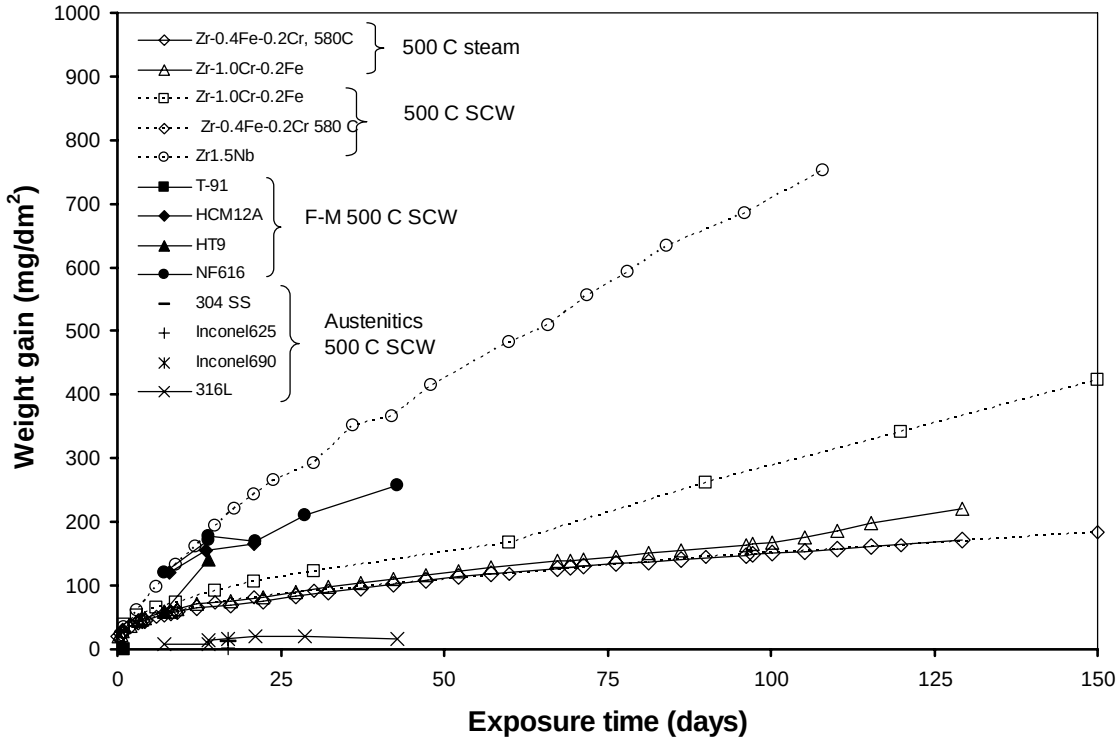

Figure 5.3: Weight gain versus exposure time for some of the zirconium based model alloys tested in this program under different autoclave conditions (SCW or steam), as indicated. Also included are corrosion results from ferritic-martensitic and austenitic alloys from other programs [2, 3].

Corrosion Data Parameters

The weight gain results in the model alloys and the reference standard alloys can be analyzed in terms of three characteristics, (which can possibly be condensed to two), illustrated schematically in Figure 5.4:

(i) **<u>the pre-transition kinetics</u>**: (red section of curve in Figure 5.4): if an oxide establishes a stable rate of growth with a protective black oxide, then the oxidation kinetics can be described by a power law of the type described in section 2.

$$w = At^n$$

where w is the weight gain in mg/dm^2, t is the exposure time, and A and n are constants, which are characteristic of the alloy.

(ii) **<u>oxide transition</u>**: it is often observed that the corrosion rate undergoes a change during oxidation, coincidentally with other changes that indicate that the oxide has lost protectiveness. In good behaving oxides, the protective layer reconstitutes itself

after the transition (blue curve) and this process repeats. The oxide thickness required to arrive at transition can be measured and serve as a measure of corrosion behavior. Some oxides do not undergo a well-marked transition and exhibit only slight slope changes (purple curve). Finally, the oxide can also become unstable at the transition and undergo loss of protectiveness (breakaway) which is our third characteristic of the corrosion process.

(iii) **loss of protectiveness in oxide** (breakaway). Breakaway is defined here as very rapid oxide growth that continues indefintely. The breakaway is interpreted as a transition in which the oxide reconstruction process is imperfect and does not re-constitute the protective layer. Breakaway can occur right at the beginning of the corrosion process or after some time (orange curves). It can also show only a moderate acceleration of weight gain such as in the green curve. In the green curve, the pre-transition (red) kinetics are not recovered, but they are somewhat slower and more controlled than the orange.

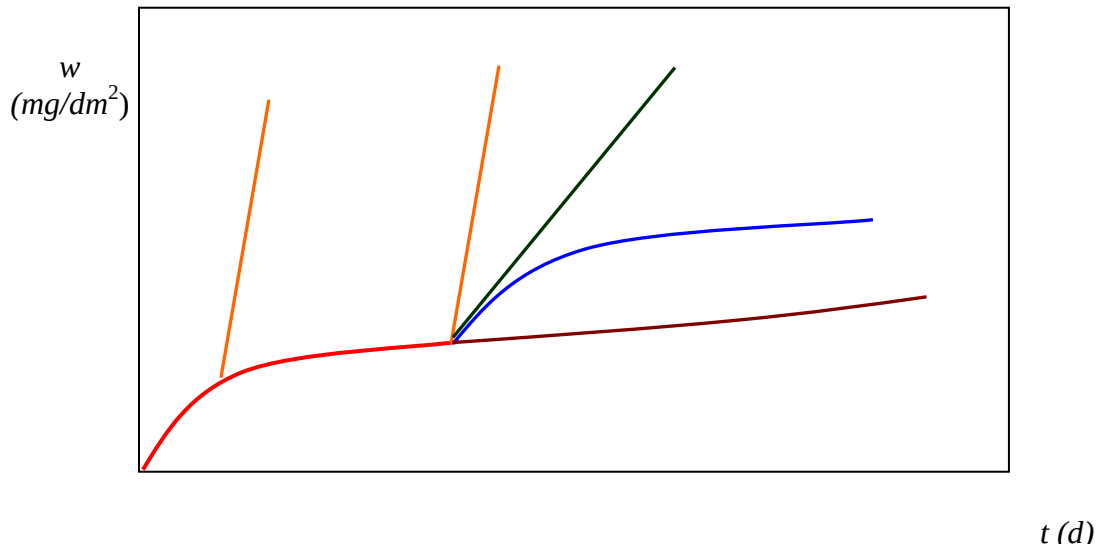

Figure 5.4: Schematic curves for illustrating different corrosion kinetics.

There are then three characteristics of the corrosion kinetics that define corrosion behavior. Items (ii) and (iii) can be considered jointly if we believe that (iii) is a transition type (ii) gone wrong. Alloying elements can influence corrosion by acting on these three different parameters and according to our hypothesis, something in the alloy microstructure causes a difference in the way the oxide grows. That is, a certain alloy microstructure implies a certain oxide microstructure, which implies a certain corrosion behavior. This work was started by specifying certain metal microstructures to investigate their role on corrosion.

Comparison of Corrosion Kinetic Behavior of Model Alloys

The model alloys were designed to investigate and isolate the effects of specific microstructures of both precipitates and solid solution elements on the corrosion process.

For precipitate forming alloys, the following effects of the microstructure on corrosion were considered:

(a) **effect of precipitate size**. The Alloy 11-14 (ZrFeCr) series was prepared with the intent of comparing precipitate size while keeping volume fraction constant and vice-versa. Alloys 11 and 13 have small precipitates while Alloys 12 and 14 have large precipitates.
(b) **effect of precipitate volume fraction**. In the same way, Alloys 11 and 12 (Zr0.2Fe0.1Cr) have a low volume fraction while 13 and 14 (Zr0.4Fe0.2Cr) have a high volume fraction. Furthermore, some of the newer alloys with higher alloying content have even larger precipitate volume fractions. Comparisons can also be made between Zr0.2Nb, Zr1.0Nb, and Zr1.5 Nb, with volume fraction increasing from 0.0 for Zr0.2Nb to higher volume fractions for the remaining alloys.
(c) **effect of precipitate type**: the comparison of the Nb alloys, high Cr alloys (alloys 21 – 24), Cu-Mo alloy (alloys 31 – 34)s and especially the newer alloys provide a variety of precipitate types.
(d) **effect of "nobility" of precipitate alloying element**. Cu is much more noble than Cr or Fe, so comparison of alloys 31 - 34 (ZrCuMo) with Cr and Cr-Fe alloys (21 - 24) should yield this information
(e) **effect of solute content**: On the solid solution side, the interest was just to examine the effect of valence on possibly creating or eliminating oxygen vacancies. => compare Nb <0.4 with Sn at various concentrations.

The ZrFeCr alloy corrosion results are quite reproducible, and show low rates of corrosion and no breakaway. The oxide thickness up until about 200 days in 360°C water is quite similar for the four alloys, i.e., no significant effect was observed as a result of the different precipitates sizes and volume fractions on the corrosion rate. Between 200 and 250 days, alloy 11 (Zr0.2Fe0.1Cr with low temperature processing) exhibits what appears to be an oxide transition, the only transition observed for the four ZrFeCr alloys.

The possible reasons for the protective behavior exhibited by these alloys (ZrFeCr) when compared to sponge Zr or crystal bar (alloys 41 and 42) are discussed below. The difference between the two alloy series (11 to 14 and 41 to 42) can be ascribed to the higher alloying element content in the ZrFe Cr alloys. The ZrFeCr alloys should have similar matrix transition element alloying contents as the solubility of Fe and Cr is in the 100's of ppm range. There are then two main differences between sponge Zr and the ZrFeCr alloys: (i) the different matrix composition (Fe/Cr in ZrFeCr vs. Fe in sponge Zr) and (ii) the presence of intermetallic precipitates in ZrFeCr.

Given the fact that no significant differences in corrosion behavior were observed between sponge and crystal bar Zr, and these exhibit significant differences in Fe content (of the level expected to be observed in the matrix of ZrFeCr alloys), it is unlikely that the difference in compositions plays a major role. The conclusion is that the precipitates play a specific role in avoiding breakaway, but not on the pre-transition kinetics as these are very similar for ZrFeCr and pure Zr. This is interesting, since there

were little differences observed for different precipitate volume fraction or different precipitates sizes. It is possible that the volume fraction of precipitates was sufficient in all of the ZrFeCr alloys to avoid breakaway. The fact that the lowest alloying element content/lowest heat treatment alloy exhibits the earliest transition indicates that differences in precipitate distribution could play a role in stabilizing the oxide layer against breakaway.

The ZrCrFe alloys in contrast, show higher rates of corrosion than ZrFeCr (except for Zr1.0Cr0.2Fe, which exhibits similar behavior as the ZrFeCr alloys). There is a marked difference in this case between the alloys of this group, with the corrosion rate and tendency to breakaway decreasing with both alloying content and presence of Fe.

The differences between these alloys and the ZrFeCr alloys are: (i) the precipitate crystal structures, (ii) precipitate volume fraction, and (iii) overall composition (reflected in precipitates composition). Since the differences between alloys 11 and 13 (cubic C15 precipitates) compared to 12 and 14 (hexagonal C14 precipitates) are not significant, it is not likely that (i) has a major effect on corrosion. Similar arguments as made for the ZrFeCr alloys lead us to place item (ii) as a possible second order effect, especially since a notable improvement was not observed for the newer higher alloying element content alloys. One hypothesis is that the presence of Fe stabilizes the precipitates against oxidation after incorporation in the oxide layer. Previous studies have shown that in order to oxidize precipitates containing Cr and Fe, it was necessary to reject the Fe into a metallic bcc Fe agglomerate which hampers the oxidation of $Zr(Cr,Fe)_2$ precipitates, compared to $ZrCr_2$. Such greater precipitate stability could allow them to play the role of preferential conduction paths for a longer time in the oxide layer and thus maintaining an orderly growth process.

In the ZrCuMo alloys, the corrosion behavior depends on the presence or absence of Mo. When Mo is present, the corrosion behavior is worse and its absence from ZrCu results in behavior similar to the better ZrFeCr alloys. ZrCuMo shows nodular corrosion, exhibits breakaway behavior and more scatter between samples. Thus, ZrCu behaves well and we do not understand why Mo has a negative effect on corrosion. In terms of precipitates, ZrCuMo has some additional small precipitates (it is the only alloy that has a bimodal precipitate distribution). We should note that the precipitates observed in ZrCu are of the type bct Zr_2Cu, and yet its behavior is similar to that of ZrFeCr, indicating that the precipitate crystal structure may not be important to the pre-transition kinetics.

The ZrNb alloys show stable oxide growth, without too much variation with Nb content, and protective behavior, without marked transitions. However, the oxide growth rate for these alloys is higher than the ZrFeCr alloys, with values of *n* around 0.4-0.45. In contrast to the ZrFeCr alloys, which have n ~ 0.2 and very straight lines up to 250 days, the ZrNb alloys show small “wiggles” in the curves, which could be interpreted as mild transitions. It is interesting to note that the ZrNb alloys with more than 0.4Nb have large number of beta Nb (and possibly ZrNbFe) precipitates in the matrix. Thus, we

have two series of alloys with large numbers of precipitates with two different transition behaviors concerning pre-transition kinetics and transition behavior.

Weight Gain Characteristic Parameters

The three measurable characteristics that we have selected for studying corrosion behavior are now discussed.

Pre-transition kinetics

The average weight gain from the short term autoclave tests (many measurements in the early stages of the corrosion experiment) were fit to a power law equation with the results shown in Tables 2.1 and 3.2. (Weight gains from individual coupons were also fit to the equation and yielded similar results.) The values of A and n are illustrated in Figures 5.5 and 5.6.

Figure 5.5 shows the values of n as calculated by fitting the corrosion curves in the protective regime, for both 360ºC and 500ºC corrosion testing. Only the alloys that exhibit sufficient protective behavior to allow a fit of the early part of the curve are shown. The vertical axis is used simply to visually separate the alloys and regimes studied. For each alloy group, various alloys and various samples are combined. The average for each group indicated in the legend is shown by a red dot. Cubic and parabolic behavior is indicated.

The results show that the values of n are in general higher during high temperature testing. The Zr-Nb alloys exhibit supra parabolic behavior (n=0.67), while the protective alloys in the ZrFeCr system show nearly cubic behavior (n=0.33), and a ZrFe-Nb alloy shows an intermediate value of n=0.43. At lower temperature, the Nb alloys still show the highest value of n (around 0.45), which is near parabolic behavior. The Zr-Sn-Nb and Zr-Sn alloys show lower values of n (0.41 and 0.29 respectively). The precipitate-forming alloys, including Zircaloy-4, ZrCrFe, ZrFeCr, and ZrCuMo, all show values of n quite close to those of pure Zr, that is, n~0.23. Figure 5.6 shows the values of A for low and high temperature testing of the model alloys. Again, the value of A in high temperature (500°C) testing are a factor 3 higher than those obtained in low temperature (360°C) tests.

In addition to the differentiation between the alloy groups, it is interesting to note that the measurements are very consistent, even considering small variations from sample to sample. This suggests that it is the overall chemical composition of the alloy that determines the value of *n*. Although not shown in the Figures, the values of *n* for Sn and Nb alloys in lithiated water are very similar to the values in pure water.

The fact that crystal bar and sponge Zr and Zircaloy-4 exhibit values of *n* close to those of ZrCrFe alloys indicates that the precipitates have a primary role in avoiding oxide growth instabilities rather than in determining pre-transition kinetics. It is also interesting to note that there is a clear distinction between the *n* values in the solid

solution forming alloys (0.3-0.5) from those in the precipitate forming ones (0.15-0.25). The conclusion here is that the pre-transition kinetics are primarily determined by the alloying elements in solid solution. Because the precipitate forming alloys have very low amounts of alloying elements in solid solution, their oxide conductivity is similar to that of Zr and likely controlled by impurities. The solid solution alloys have kinetics that are dependent on the amount and the type of solute element.

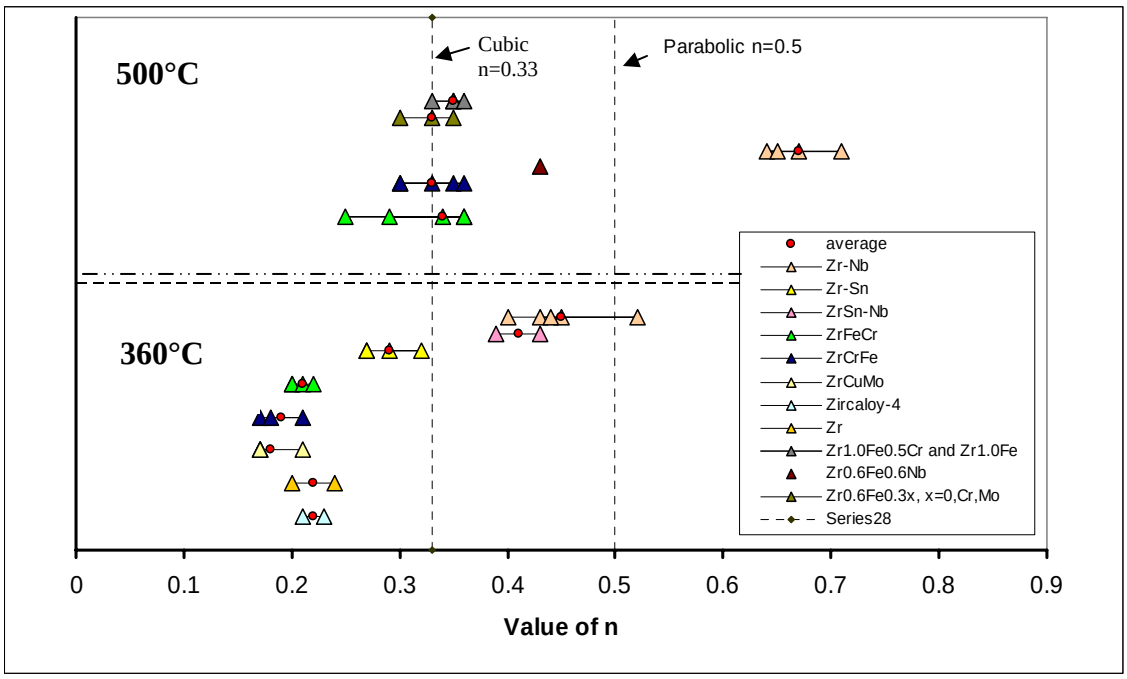

Figure 5.5: Values of *n* for the different alloys and environments. The vertical axis has no meaning and is simply for displaying the values separately. In the upper part of the plot, the values for 500°C SCW and steam and in the bottom are the values for 360°C testing.

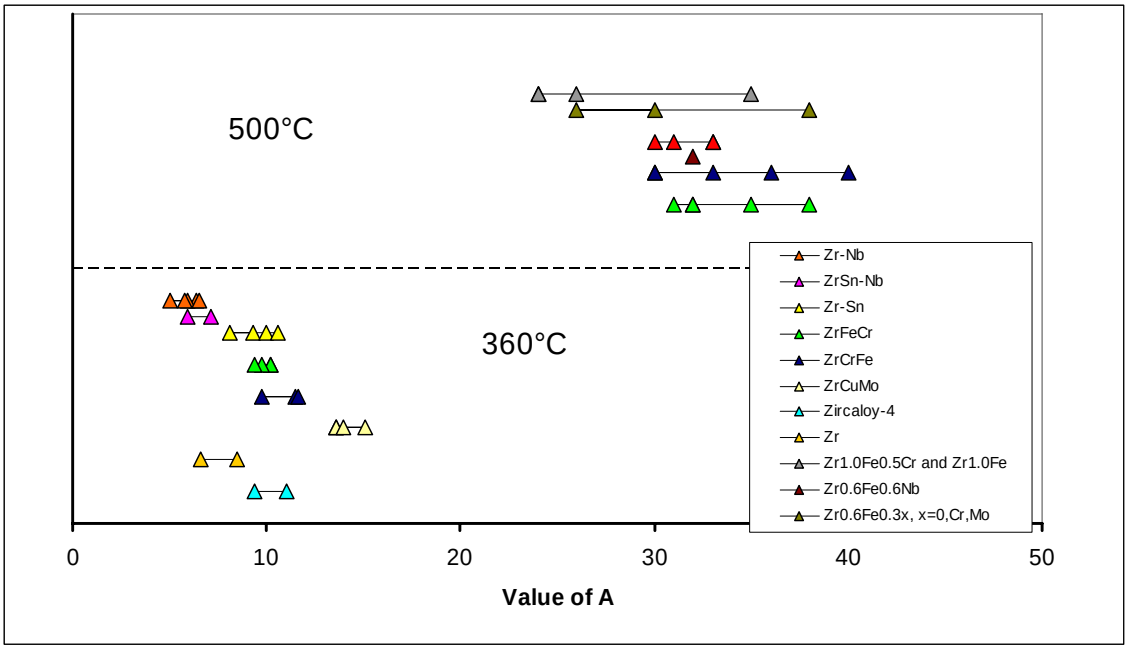

Figure 5.6: Values of *A* for the different alloys and environments. The vertical axis has no meaning and is simply for displaying the values separately. In the upper part of the plot, the values for 500°C SCW and steam and in the bottom are the values for 360°C testing.

Deviation from Parabolic Kinetics

In oxide growth limited by oxygen transport in a protective layer, the growth kinetics are parabolic (n=0.5). After an initial transient (as the film is established), the rate limiting step (RLS) should be some form of transport through oxide, (rather than interfacial reaction) because the oxide growth rate is observed to decrease continuously as the protective oxide thickness increases. Further evidence of this is given by the lack of dependence of corrosion rate on oxygen pressure. If it is accepted that transport through the oxide is the RLS and if this rate limiting step achieved by simple diffusion through a homogeneous medium, with fixed boundary conditions, then the parabolic law is obtained.

Since the deviations from parabolic law are all towards lower values of *n* (lower corrosion rates) a diffusion controlled process with sub-parabolic kinetics implies some form of slowed down or “hampered” diffusion. It is interesting to discuss the mechanisms of departure from parabolic law, as this allows one to discuss the ways in which the different alloys can influence corrosion behavior.

The first question is whether diffusion occurs through the bulk of the oxide or through the grain boundaries. Cox and co-workers [4] have shown that there is a double profile of oxygen, one very close to the surface and one extending far into the oxide. Using a diffusion equation solution, Cox et al. derived an activation energy for the far profile which was approximately 1-1.4 eV. They compared this with other measurements of

vacancy diffusion in zirconia and found that in bulk zirconia the activation energies are much higher (> 3 eV). They interpreted this as indicating that the diffusion occurred by a grain boundary diffusion mechanism. A simple calculation of the oxygen flux necessary to sustain the advancement of the oxide layer shows that the activation energy of 1-1.4 eV is that responsible for the layer advance.

However, the measurement in bulk zirconia was in stoichiometric ZrO_2, and thus the activation energy includes both migration and formation energy. In the sub-stoichiometric zirconia layers, the vacancies are already present and thus the activation energy is constituted only of the migration energy, which could then be equated with the activation energy measured by Cox et al. The exact migration mechanism could be either bulk or grain boundary diffusion and both diffusion mechanisms are considered in the following.

Another question is the identity of the migrating species. Because the oxide is sub-stoichiometric, the oxygen vacancy is the defect considered to be the transporting species. One question arises as to what types of defects are formed in the growing oxide layer, i.e. how is charge compensated. If a vacancy gradient exists, as assumed by the parabolic model, then the number of electrons in the oxide needs to have a similar gradient to allow for charge compensation.

Mechanisms for Deviation from Parabolic Law.

Various ideas have been invoked in the literature to explain the deviation from parabolic behavior:

1. **Grain size gradient** [5]. This mechanism assumes grain boundary diffusion. As the grains grow, there is less area for oxygen to travel through. If the increase in grain size is linear with oxide thickness, a cubic law is obtained. With other dependences on thickness, other values of n would appear. In favor of this hypothesis is that (i) the grain size is observed to increases in the better performing commercial alloys, (ii) the grain size variation necessary for this increase would have to be substantial, (if the corrosion rate decreases by a factor of 2 so should the grain boundary density, and thus the grain size decrease by this factor with distance from the oxide metal interface). Such a large change is not seen.
2. **Grain boundary structure:** A more subtle grain boundary effect could be possible if the grain boundary structure changed with oxide thickness, so that it is more or less permeable to diffusion. No obvious reason exists for such a continuous change, however.
3. **Cracking**: Presence of lateral cracks, the density of which increases with oxide thickness. In this mechanism, diffusion occurs through the bulk of the oxide. As stresses develop, the density of lateral cracks increases. Because the vacancies cannot go through the cracks, the oxygen flow is diminished. Again a linear increase would cause the cubic law, and other functions lead to other values of *n*. (pro: we observe lateral cracks frequently in the oxides; con: oxides that crack more easily

would have lower corrosion rates, which is contrary to observation. Also, the cracking observed in the oxide occurs at or after the transition and not throughout the oxide)

4. **Stress effect on diffusion**. Stresses accumulate in the oxide as it grows, so that the lattice is "squeezed" and migration energy increases, decreasing the flow of oxygen In favor of this idea is that compressive stresses are known to exist in the oxide layer during corrosion, but against is that a simple calculation shows that the elastic energy calculated by assuming the maximum possible stress in the elastic regime (σ_y) is small (on the order of 0.01 eV/atom) compared to the migration energy (~ 1 eV/atom).
5. **Thickness of barrier layer**: It is well known from different measurements (lithium uptake[6], and Electrochemical Impedance Spectroscopy (EIS) as in the present work) that in the pre-transition regime there is a double layer of oxide, one more protective (often called the barrier layer) and one more porous outer layer. If we denote X=Protective/Total oxide thickness ratio and X does not change in the pre-transition regime, the parabolic regime is again found. If it is assumed that X changes as the oxide grows, then again almost any kinetics could be found. In that case, the $W=At^n$ curve would have a factor X that could create a new effective *n*. For the mechanism to yield *n* <0.5 X would have to increase with thickness. Such a layer has been observed, but it is not obvious why X would change with thickness.
6. **Electron transport control**. In this case, we would assume that vacancy migration adjusts itself to the availability of electrons to allow for charge compensation. Fromhold [7] gives an expression for the deviation from parabolic law in terms of an exponential for a very simple case. If this is the rate limiting step, or if it alternates with vacancy diffusion as RLS, then could explain different kinetics. In favor of this idea is that this can provide a link with precipitate and precipitate distribution; but is it possible to accumulate space charge across oxide?
7. **Role of suboxide**: It is clear that a significant amount of oxygen is absorbed by the metal ahead of the advancing oxide front, as has been demonstrated in this study. Clearly, the more oxygen is lost to the metal, the slower will the oxide front advance. Such slowing down will be proportional to the length of the sub-oxide region. The model would predict that this oxygen-rich region would increase with time and that slower moving oxides would have a greater oxygen rich region. The measurements ahead of the oxide front show more oxygen in the fast moving oxides, but this is the profile associated with precipitation of oxides ahead of the front (>0.3). It is not clear how far the 0.3 plateau extends into the metal. Oxygen is in fact lost to the metal and different alloys have different profiles, but the amount of oxygen lost appears relatively small to account for the slowing down.

Mechanism number 1 can be eliminated based on observations. If the grain increase is not enough, it cannot work. Mechanisms numbers 2 or 3 appear unlikely on simple experimental and observation grounds.

If we now compare the different behavior of the classes of model alloys, we can discuss further these models. Since Zr-Nb has near-parabolic kinetics, it could be possible to study microstructure differences between these oxides and those in the precipitate alloys.

It is noted that pure Zr, in the instances when it has low corrosion rate at the beginning, (i.e. when the weight gain does not increase suddenly right at the start) has *n* in the range about 0.2-0.25, which is the same as that of the ZrFeCr, ZrCrFe, alloys. This, it seems reasonable to assume that the presence of precipitates does not influence the kinetics of pre-transition.

Since Sn also has a higher *n* than 0.2, it seems reasonable to assume that alloying elements in solid solution control pre-transition behavior. It is also interesting to note that of the ZrNb alloys, the lowest corrosion rate was seen in the only alloy with a composition below the solubility limit (Zr0.2Nb). This again points to the role of solid solution elements on the pre-transition behavior. We also note that the corrosion rate of Zr0.2Nb was similar to that of Zr0.4Sn0.2Nb; note also that Zr0.4Sn0.4Nb behaves like Zr0.4Nb, which suggest specifically that Nb content controls pre-transition kinetics. One possible hypothesis is that in the absence of solid solution elements to change the valence of the oxide and create vacancies, the oxide grows very slowly in the ZrFeCr, Zr, etc. So Sn and Nb would create vacancies in ZrO_2 and allow the transport through the oxide to be performed in a faster, but perhaps more orderly, manner. The difference in behavior of Zr and precipitates alloys would be due to the latter being able to avoid instabilities that would lead to the orange curve (Figure 5.4). This would explain why the precipitate elements have lower *n*, but would not explain why Zircaloy also had *n* ~0.2 (since Zircaloy contains Sn).

In summary, it appears that the main link between alloy microstructure and composition with pre-transition corrosion rate stems from the amount of solute in solid solution, and from the valence of this element. The evidence above would appear to indicate that the overall chemistry of the solid solution controls the pre-transition behavior, such that elements such as Nb and Sn increase the transport properties of the oxide. For the precipitate forming elements, the amount in solid solution is very small, and the pre transition rate is likely controlled by impurities or by the small amount of alloying element content.

One key question is: beyond determining mechanisms, is it important to know why the kinetics are not parabolic? It would appear not, since the greatest influence on the overall corrosion rate appears to be the thickness at first transition and the ability to avoid corrosion breakaway. In this case the precipitates formed appear to enhance oxide stability, as discussed below.

Oxide Transition

The oxide transition is defined as the thickness at which the corrosion weight gain shows a sudden increase, as shown in Figure 5.1. The thicknesses at transition can be quite different for the various alloys [8]. The transition is normally interpreted as a more or less “sudden” event that causes the oxide to lose its protective character and allows water to penetrate the oxide layer, possibly down to the metal region.

As the oxide grows, the metal is transformed into zirconia, which entails an increase in volume of approximately 1.56. The great majority of this volume increase is accommodated in the vertical direction as 1 micron of oxide results in approximately 1.56 microns of oxide. It is difficult however, to account exactly for this volume increase, as the error in the measurement of oxide thickness is not much smaller than 5%, and a few % difference in the accommodation of these strains would lead to large stresses. It is known in fact that stresses accumulate in the oxide layer and also that stresses are higher in alloys that show earlier transition (Zircaloy-4) compared to later transition (M5)[9, 10]. It is also likely that a stress gradient exists in the oxide layer, with higher stresses near the oxide-metal interface. Typically, stresses on the order of 2 GPa have been measured in the oxide layers. It is possible that the accumulation of the stresses differs among the different alloys, due to different "phase transformation tensors" (relationship between orientation of the film during transformation of Zr into ZrO_2.).

It should be noted that transitions in the classical sense are not seen in some of the alloys. In the set of alloys studied, Zircaloy 4 exhibited a clear transition, as did the Zr-Sn alloys. The ZrFeCr alloys have in general not yet exhibited a clear transition, (although alloy 11 may be starting). None of the ZrNb alloys have yet shown a marked transition. So, preliminarily, we associate a marked transition with the presence of Sn. Some of the oxides however have exhibited breakaway after long exposures.

Mechanisms of oxide transition

1. Stress accumulation breaks oxide. In this case, it is assumed that the lateral stresses that accumulate reach a critical point and break the oxide. If vertical cracks are created, water has access to the oxide-metal interface and the corrosion rate increases. Although it is known that in-plane compressive stresses accumulate, which would tend to cause lateral cracks. The presence of cracks in and of itself, would cause little effect on the permeability of this oxide layer. To cause the oxide to lose protectiveness it would be necessary to create vertical cracks. This could happen for example by one of the processes shown in Figure 5.7: (a) shearing a block of the oxide, (b) blistering or (c) surface instabilities) that would allow a compressive stress to cause vertical cracks. However there are reasons to question the three processes illustrated below on either theoretical or experimental grounds: no blistering is seen during corrosion at small oxide thicknesses, no vertical cracks are seen in general and no cracks are seen associated with the ends of lateral cracks; finally surface instability (which predicts a shear stress as result of the propagation of an interface instability) only allows for about 200 Mpa as a maximum of the stresses it can induce, which is small compared to the stresses accumulated.

Thus, although stresses accumulate in oxides and stress accumulation may be different among alloys, it is difficult to see how the stresses that are present in growing oxides would cause transition.

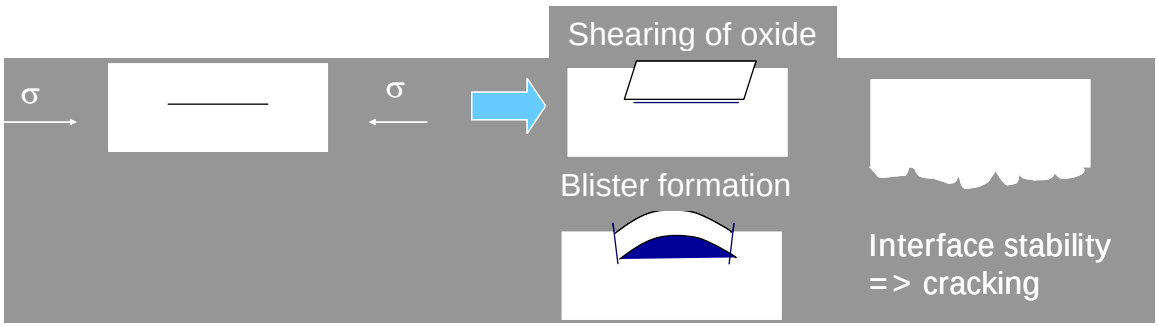

Figure 5.7 Stress accumulation leading to oxide cracking.

2. Porosity increases and percolates; During oxide advancement, new grains are constantly created, with varying interfaces. At these interfaces, small grain boundary mismatches can create little "wormholes" at grain boundaries, which then allow access of water once the porosity is interlinked. Conceivably, the density of these wormholes (or pores) could increase with oxide thickness as a result of preferential attack at grain boundaries. If the porosity increases with oxide thickness then at some critical pore density a continuous path will be established from the oxide-metal to the oxide- water interface, a condition known as *percolation.* Cox and co-workers have measured oxide porosity, and others such as Godlewski and Pecheur, as well as Barberis [6, 11-13] have found that the external layer at least is porous. However the porosity exists in the outer layer, not in the barrier layer, which controls diffusion. In addition, there is no obvious reason for the porosity to continuously increase with continued oxide growth. Thus, because of the above, it is also not clear how this mechanism could cause transition or breakaway.

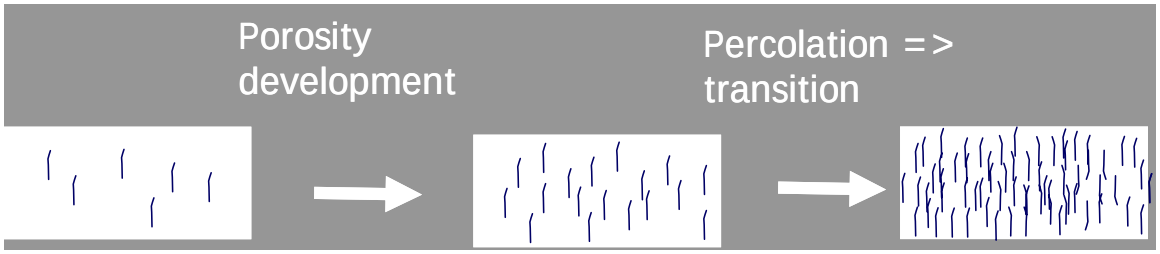

Figure 5.8 The percolation mechanism for the transition.

3. Mixed mode transition [14]: This mechanism combines a gradual process (porosity development) with a sudden process (cracking) and is based on the fact that if porosity exists, percolation can be reached with lateral cracking. In this idea, porosity is developed during the formation of the grains and remains constant thereafter, although at different stages of the oxide growth process we could have different densities of pores being created at the O/M interface. The crucial step is that while this constant porosity does not change with thickness at a given position, the onset of lateral cracks could push that porosity over the percolation condition.

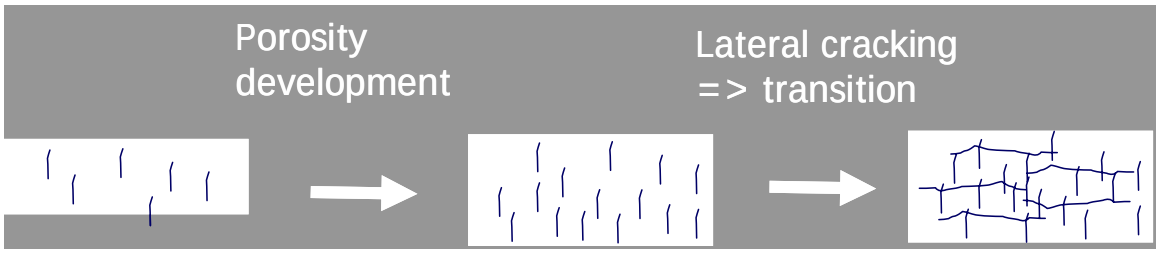

Figure 5.9: The mixed mode mechanism for oxide transition/breakaway.

If this mechanism works, then oxides that have larger grains and with less grain to grain mismatch should exhibit les tendency to breakaway. This is in fact the case with the commercial alloys we have studied. The grain size measured with synchrotron radiation is however similar for the alloys studied. However the differences observed in texture formation cause differences in oxide behavior, such that an orderly process of formation of well aligned oxide grains leads to better resistance to breakaway.

This then poses the question as to what in the alloy causes orderly well-oriented oxide growth with large grains. It could be argued that the slowness of growth allows for oxide to rearrange itself which would allow better aligned growth. But, in fact some of the oxides with low *n* are more susceptible to breakaway (pure Zr for example), which suggest slow and *stable* oxide growth is needed. If the precipitates and alloying elements in the oxide layer allow for equalization of current around the surface (metal grain to metal grain or possibly causing instabilities in oxide growth to be flattened), then this will help delay the transition.

In summary, the mixed mode transition model seems to be a good working hypothesis for the transition mechanism.

Breakaway Susceptibility

The most obvious difference in the behavior of the alloys comes from their different breakaway behavior. Some alloys exhibit protective behavior until very long exposure times, while others show non-protective behavior right from the beginning. The key questions to ask are what in the oxide re-growth process causes breakaway and what causes the difference in breakaway susceptibility between the various alloys.

These can be two separate but related questions. One relates to what goes wrong in the transition to breakaway and the other relates to the consequences of this event.

There are various interesting points about the breakaway susceptibility. Some alloys, such as pure Zr, go for some time before they undergo breakaway. That is, they form a black protective oxide, with similar kinetics as other protective oxides and then undergo breakaway. Thus the process of forming a protective oxide appears to be irreversibly disturbed. In some way the oxide reaches a bifurcation and takes the road of fast kinetics

never to return. Once breakaway occurs it appears to be irreversible. This implies that the oxide formed causes the kinetics to be fast. Presumably, if the oxide was removed and the process restarted, the new oxide would have a chance to reform correctly. Finally, very small differences in composition make large differences in corrosion behavior.

Microstructural Features of Protective Oxides

In section 4, the microstructural features of a protective oxide compared to those of a non-protective oxide were discussed, and are summarized here.

1. The oxide-metal interface in the protective oxides showed the presence of a sub-oxide phase, which is an ordered solid solution of oxygen in Zr ahead of the oxide front. This layer was a factor of 10 thicker in the oxides formed in 500ºC testing than in the oxides formed in 360ºC testing.

2. Also at the oxide-metal interface, the following strong orientation relationship was seen $[10\bar{1}0]_{hcp}//[002]_T//[020]_M$. The key to establishing the strong relationship between $[020]_M$ and $[10\bar{1}0]_{hcp}$ planes is the presence at the interface of the $[002]_T$ precursor phase. This highly oriented tetragonal phase forms ahead of the oxide layer and is present in the protective oxides and absent in the non-protective ones.

3. As a result of this, the ratio of the intensities of the $[020]_M$ to $[002]_M$ peaks was higher in the bulk of the protective oxides than in the non-protective oxides.

4. In addition, differences were seen in the thickness-averaged crystallographic texture of the protective and non-protective oxides. It appears that a more orderly growth and well oriented oxides decrease the tendency for corrosion breakaway.

Following the model developed for normal oxide growth we can then try to explain breakaway. Since at transition small tetragonal equiaxed grains form which later transform to monoclinic, possibly the critical point is the proper transformation of tetragonal into monoclinic. Comparing Zr alloy corrosion behavior with Hf, Hf is quite a bit more protective than Zr. One important difference in the two oxide systems is the fact that Hf forms only one phase, and Zr forms two. It is possible that the transition from one phase to the other causes the instabilities we observed. When that transformation occurs properly, i.e. when enough grains exist of the proper orientation or when the highly oriented tetragonal phase forms and leads to new aligned oxide then breakaway is averted. It is possible that the volume increase from tetragonal to monoclinic plays a role (although it has to be better evaluated).

The main conclusions as to relating the microstructure of the alloys and of the oxides with the corrosion rate are:

1. The microstructure in the protective oxides described above, provides a better alignment and likely induces less stress accumulation, and thus delays the onset of breakaway or loss of protectiveness.

2. This microstructure associated with protective oxides is present during both 360ºC and 500ºC testing and in the same alloys. Thus, the protection mechanism is likely the same at both temperatures.

3. The presence of precipitates is seen as crucial at avoiding breakaway, by allowing a steady transport of electrons through the oxide, (since the precipitates are not oxidized in the barrier layer), thus avoiding large lateral differences in corrosion rate, and enhanced oxide breakup.

The proposed mechanism for loss of protectiveness, (a combination of cracking and porosity percolation) can likely explain the experimental results.

Conclusions

A detailed study has been conducted to address the issue of susceptibility of Zr alloys to uniform corrosion in the proposed supercritical water reactor and of the specific role of alloying elements. Thirty model alloys were corrosion-tested for periods over 400 days in 360ºC water (as well as limited testing in lithiated water), from 150 to over 300 days in 500ºC supercritical water and a wide range of corrosion behavior was observed. The general agreement between the three high temperature tests was quite good. In particular little difference was seen between the results from static and dynamic autoclave testing. The results from lower pressure static testing agreed with the supercritical water results but showed slightly less oxide growth. Since the rankings of the alloys were preserved from test to test, it is possible the steam test could serve as a preliminary screening test for supercritical water behavior.

1. Corrosion tests for the model Zr alloys showed a wide variety of corrosion resistance depending on the alloy composition during both 360ºC and at 500º testing. These differences manifested themselves in the different values of A and n obtained for the different alloys and in the different tendencies for breakaway.

2. In comparison with other alloys being considered for the SCWR, the Zr alloys showed higher corrosion rates than austenitic alloys, and lower corrosion rates than ferritic-martensitic and 12Cr steels.

3. Significant concerns exist in terms of creep rates, and other properties, but this research indicates that proper alloying additions induce protective oxide growth in model Zr alloys, such that from the corrosion point of view they should be considered as possible candidate materials for application in the supercritical water reactor.

The oxides were also characterized to determine the oxide structures associated with protective and non-protective behavior and the conclusions are:

4. Characteristic differences exist in the oxide-metal interface regions of protective as compared to non-protective oxides. In particular the presence of two interfacial oxide phases, a highly oriented tetragonal phase and a sub-oxide phase was associated with protective behavior uniform corrosion.

5. The overall crystallographic texture of oxides also showed clear differences between protective and non-protective oxides. The growth direction of the oxides was similar but the distribution of the lobes was considerably more anisotropic in the non-protective oxides than in the protective ones.

6. The protection mechanisms and the mechanisms of transition/breakaway were discussed and the differences between alloys are rationalized in terms of mechanistic models.

References

[1] A. Motta, A. Yilmazbayhan, M. G. d. Silva, R. J. Comstock, G. Was, J. Busby, E. Gartner, Q. Peng, Y. H. Jeong, and J. Y. Park, "Zirconium Alloys for Supercritical Water Reactor Applications: Challenges and Possibilities," Journal of Nuclear Materials, vol. submitted, (2006).

[2] G. S. Was and T. R. Allen, "Time, Temperature, and Dissolved Oxygen Dependence of Oxidation in Austenitic and Ferritic-Martensitic Alloys in Supercritical Water," International Congress on Advances in Nuclear Power Plants, Seoul, Korea, (2005), vol.

[3] S. Teysseyre, J. McKinley, and G. S. Was, "Latest Results on SCC and Corrosion of Austentic and Ferritic-Martensitic Steels in SCW at University Of Michigan," 4th SCWR Information Exchange Meeting, Pittsburgh, (2004), vol.

[4] B. Cox and J. P. Pemsler, "Diffusion of Oxygen in Growing Zirconia Films," Journal of Nuclear Materials, vol. 28, (1968), 73-78.

[5] G. P. Sabol and S. B. Dalgaard, "The Origin of the Cubic Rate law in Zirconium Alloy Oxidation," Journal of the Electrochemical Society, vol. 122, (1975), 316.

[6] D. Pecheur, J. Godlewski, P. Billot, and J. Thomazet, "Microstructure of Oxide Films formed during the waterside corrosion of the Zircaloy cladding in Lithiated environment," 11th International Symposium on Zr in the Nuclear Industry, Garmisch-Partenkirchen, (1995), ASTM, vol. STP 1295, 94-113.

[7] A. T. J. Fromhold, Theory of Metal Oxidation, vol. 9. New York: North-Holland, 1976.

[8] A. Yilmazbayhan, A. T. Motta, R. J. Comstock, G. P. Sabol, B. Lai, and Z. Cai, "Structure of Zirconium Alloy Oxides formed in pure water studied with Synchrotron radiation and optical microscopy: relation to corrosion rate," Journal of Nuclear Materials, vol. 324, (2004), 6-22.

[9] J.-L. Bechade, R. Brenner, P. Goudeau, and M. Gailhanou, "Determination des contraintes internes dans une couche de zircone par diffraction des rayons X et par une approche micromecanique: influence de l'anisotropie thermoelastique," Revue de Metallurgie, (2003), 1151-1156.

[10] J.-L. Bechade, R. Brenner, P. Goudeau, and M. Gailhanou, "Influence of temperature on X-ray diffraction analysis of ZrO_2 oxide layers formed on zirconium based alloys using a synchrotron radiation," Proceedings of the 6th European Conference on Residual Stresses, Jul 10-12 2002, Coimbra, Portugal, (2002), Trans Tech Publications Ltd, vol. 404-407, 803-808.

[11] P. Barberis and A. Frichet, "Characterization of Zircaloy-4 oxide layers by impedance spectroscopy," Journal of Nuclear Materials, vol. 273, (1999), 182-191.

[12] J. Godlewski, J. P. Gros, M. Lambertin, J. F. Wadier, and H. Weidinger, "Raman Spectroscopy Study of the Tetragonal-to-Monoclinic transition in Zirconium oxide scales and determination of overall oxygen diffusion by nuclear microanalysis of ^{18}O," 9th International Symposium on Zr in the Nuclear Industry, Kobe, Japan, (1991), ASTM, vol. STP 1132, 416-436.

[13] J. Godlewski, "How the Tetragonal Zirconia is Stabilized in the Oxide Scale that is Formed on a Zirconium Alloy Corroded at 400 C in steam," 10th Int.Symp. on Zr in the Nuclear Industry, (1994), ASTM, vol. STP 1245, 663-686.
[14] R. G. Lott; personal communication to A. Motta, 2004